Seismic fragilities of single-column highway bridges with rocking column-footing

Yazhou Xie[1], Jian Zhang[2], Reginald DesRoches[1], and Jamie E. Padgett[1]

[1]*Department of Civil and Environmental Engineering, Rice University, Houston, TX 77005, USA*
[2]*Department of Civil and Environmental Engineering, University of California, Los Angeles, CA 90095, USA*

Abstract

Rocking isolation has been increasingly studied as a promising design concept to limit the earthquake damage of civil structures. Despite the difficulties and uncertainties of predicting the rocking response under individual earthquake excitations (due to negative rotational stiffness and complex impact energy loss), in a statistical sense, the seismic performance of rocking structures have been shown to be generally consistent with the experimental outcomes. To this end, this study assesses, in a probabilistic manner, the effectiveness of using rocking isolation as a retrofit strategy for single-column concrete box-girder highway bridges in California. Under earthquake excitation, the rocking bridge could experience multi-class responses (e.g., full contacted or uplifting foundation) and multi-mode damage (e.g., overturning, uplift impact, and column nonlinearity). A multi-step machine learning framework is developed to estimate the damage probability associated with each damage scenario. The framework consists of the dimensionally consistent generalized linear model for regression of seismic demand, the logistic regression for classification of distinct response classes, and the stepwise regression for feature selection of significant ground motion and structural parameters. Fragility curves are derived to predict the response class probabilities of rocking uplift and overturning, and the conditional damage probabilities such as column vibrational damage and rocking uplift impact damage. The fragility estimates of rocking bridges are compared with those for as-built bridges, indicating that rocking isolation is capable of reducing column damage potential. Additionally, there exists an optimal slenderness angle range that enables the studied bridges to experience much lower overturning tendencies and significantly reduced column damage probabilities at the same time.

KEY WORDS: highway bridges, rocking, overturning, column damage, fragility estimate, machine learning

1. Introduction

The rocking behavior of bridge structures on shallow footings when excited by earthquake motions has been recently considered as a potentially beneficial seismic design concept [1–6]. The rocking motion in such systems involves the sliding and uplifting of footings, with significant nonlinear behavior expected from the supporting soils. As a result, the induced settlement and permanent rotation of the footings remain difficult to predict and may cause large permanent deformation response of the bridges. Seismic performance of rocking bridges with shallow footings is highly susceptible to the competence of the supporting soils [7,8].

To take advantage of the rocking concept and avoid the complexity associated with supporting soils, this study investigates an alternative rocking isolation strategy that features a detached rocking interface between the bottom of footing and the rigid support underneath (Fig. 1), a system whose seismic response has been studied using dimensional analysis previously [9]. The promise of the proposed system can be analogous to unanchored rigid structures such as water tanks, tombstones, and ancient temples, which have demonstrated exceptional seismic performance during past earthquakes [10]. However, unlike rigid structures, the relatively tall and slender rocking bridges require the consideration of inherent column flexibility. The coexistence of column oscillation and footing rocking complicates the dynamics of the rocking system [9].

Considerable past studies have investigated the rocking dynamics of free-standing rigid blocks, rigid-rocking frames, and coupled structures [11–18]. Developed from Housner's inverted pendulum model [11], the dynamic responses of rigid rocking systems when subjected to pulse-type motions were investigated in depth. Critical concerns have been placed on the energy dissipation models at impact [19–22], the uplift and overturning conditions [12,13], and the development of rocking spectra (i.e., the maximum base rotations) [23]. On the other hand, previous experimental studies have indicated significant uncertainties and variabilities in terms of the rocking responses under

individual earthquake motions [24–27].

Another area of research work on rocking structures has focused on the dynamic performance of flexible rocking oscillators [9,25,28–33]. Relative studies have investigated the following: (1) the rocking impact mechanism and transition between rocking phase and full contact vibration phase [31,32]; (2) the dynamic interplay of column vibration and foundation rocking [9]; and (3) the ground motion intensity measures (*IMs*) that cause significant rocking amplitudes [9,30]. However, seismic responses of flexible rocking oscillators are more complex due to the extra column vibrational mode. Experimental studies have confirmed that the entire time history responses of flexible rocking oscillators are very sensitive to modeling uncertainties and test setup [25,33–35].

Recently, relevant works have assessed the seismic performance of rocking structures in a probabilistic way [30,36–40]. Fragility curves that estimate overturning probability and rotation demand were developed by Dimitrakopoulos and Paraskeva [36] for rigid rocking structures by using bivariate *IMs*. Their study concludes that the rocking overturning tendency depends primarily on the velocity characteristics of ground motions. Further, the study from Giouvanidis and Dimitrakopoulos [37] have identified that the maximum rotation response of free-standing blocks correlates stronger to the time intervals during which the ground motion uplifts the block. A different fragility model that involves more *IMs* such as the peak ground acceleration (*PGA*), peak ground velocity (*PGV*), and arias intensity (*I_A*) has been developed for rigid rocking bodies by applying the Bayesian updating approach [40]. Response surface models and stepwise regressions were used in Sichani et al. [39] to develop a two-layer probabilistic seismic demand model of concrete dry cask structures that are expected to slide, wobble, and rock in a seismic event. Moreover, Bachmann et al. [38] conducted a statistical comparison between experimental and numerical responses of a rigid rocking oscillator to two ensembles of ground motions. Their study confirmed that despite the difficulty of reproducing experimentally measured response time history under a given motion, the cumulative distribution functions (CDFs) of the rocking demand produced by numerical analyses are very close (i.e., within 90% of confidence intervals) to experimental CDFs. This study motivates the current work to estimate the seismic demand and fragility of flexible rocking structures probabilistically, which has yet to be explored systematically.

To this end, the present work focuses on the seismic fragility estimates of the rocking bridges through the use of surrogate models and machine learning tools. The bridge class designed with rocking isolation is selected as the aging single-column box-girder concrete bridges in California. Dynamics of the sample rocking bridges demonstrate a multi-class and multi-mode damage scenario when subjected to different ground excitations. A probabilistic analysis framework is formed to incorporate modeling and response uncertainties stemming from ground motions, material properties, and bridge geometries. To address the complex rocking dynamics and the associated multiple classes and modes of damage, a multi-step machine learning methodology is developed. The probabilities of uplift, impact and column damage, and overturning are calculated using the total probability theorem, which combines the response class probabilities (e.g., overturned or not) and conditional damage probabilities (e.g., column damage given the rocking condition). Furthermore, the rationale and requirement of rocking isolation design is investigated by comparing the fragility estimates of rocking bridges with that of as-built bridge columns.

2. Rocking isolation, analytical modeling, and dynamic performance

2.1 Rocking isolation and analytical modeling

For single-column bent bridges (Fig. 1(a)), rocking isolation is realized by designing a small footing that is monolithically connected with the column, whereas the column-footing system is detached from the rigid support underneath (Fig. 1(b)).
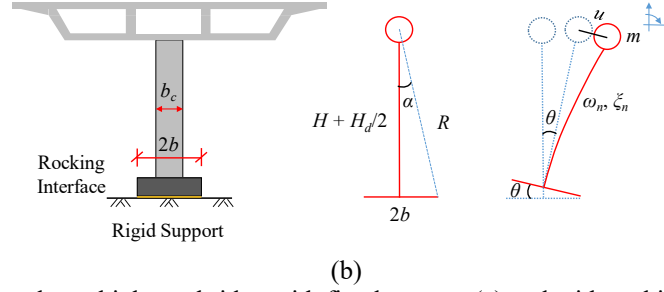

(a)

(b)
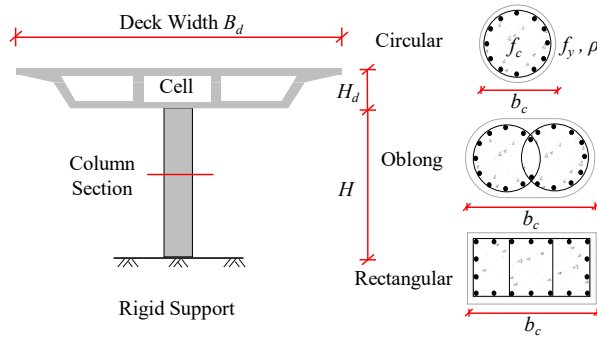
Fig. 1 Single-column highway bridge with fixed support (a) and with rocking isolation (b)

A sample calculation is conducted with respect to the rocking system shown in Fig. 1(b) by assuming: (1) a span length of 32 m, a deck width of 10 m, a column height of 6.6 m, and a circular column section with a diameter of 1.5 m; and (2) a square plan section for the footing with a width of 3 m and a height of 1 m. The sample calculation indicates that the column and footing masses are about 6% and 4% of the participating weight from the deck, respectively. As such, the much smaller column and footing masses can be neglected and the rocking bridge can be idealized as a two degree of freedom (DOF) system (Fig. 1(b)). Such an idealization has also been utilized in previous studies for the investigation of flexible rocking oscillators [9,28,30,32,41]. The proposed model consists of a point mass on an axially rigid yet translational flexible column that is connected to the rigid footing at the bottom. The system variables are the column translational drift, u and the rigid body rotation of the footing, θ. As is noted in Fig. 1(b), the deck mass inertia is represented by a concentrated mass m, the deck height is H_d, and the column is considered to have a height of H, a base width of $2b$, a vibrational natural frequency of ω_n, and a damping ratio of ξ_n. Two additional assumptions for the analytical model are: (1) the friction at the rocking interface is sufficient to avoid sliding of the rocking bridge at the base; and (2) a rigid-to-rigid pointwise contact is considered in the rocking phase between the footing and the support.

The nonlinear equations of motion (EOMs) of the analytical system at the rocking phase can be derived following Lagrange's equation of energy equilibrium [9]:

$$\ddot{\theta}[H_e^2 + b^2 - \text{sgn}(\theta)2bu + u^2] + H_e\ddot{u} - 2\dot{\theta}\dot{u}[\text{sgn}(\theta)b - u]$$
$$-g[H_e\sin\theta - \text{sgn}(\theta)b\cos\theta + u\cos\theta] = -\ddot{u}_g[H_e\cos\theta + \text{sgn}(\theta)b\sin\theta - u\sin\theta] \qquad (1)$$

$$\ddot{\theta}H_e + \ddot{u} + 2\xi_n\omega_n\dot{u} + \dot{\theta}^2[\text{sgn}(\theta)b - u] - g\sin\theta + \omega_n^2 u = -\ddot{u}_g\cos\theta \qquad (2)$$

where H_e is the effective height that equals to $H+H_d/2$; g is the gravitational constant; $\ddot{u}_g$ is the acceleration magnitude of the input ground motion; and $\text{sgn}(\theta)$ is the signum function of the footing rotation θ. Note that the rocking phase system EOMs shown in Eqs. (1) and (2) are triggered only when the uplift condition is met, namely when the overturning moment due to external loads exceeds the resisting moment provided by gravity:

$$\mp m(\ddot{u}_g + \ddot{u})H > mg(b \mp u) \qquad (3)$$

When the condition shown in Eq. (3) is not satisfied, the equation for a one-DOF oscillator can be used to characterize the system dynamics at the full contact phase:

$$\ddot{u} + 2\xi_n\omega_n\dot{u} + \omega_n^2 u = -\ddot{u}_g \qquad (4)$$

Eqs. (1) to (4) capture the dynamics of the rocking system in two different phases: rocking phase and full contact phase. However, at each time when the rocking footing contacts the rigid support, impact happens at the interface with some kinematic energy loss. Such energy loss can be captured in a classic manner by assuming the duration of impact is instantaneous and the energy loss is non-continuous. Relevant impact models include the preservation of horizontal momentum [28], the vertical velocity loss [31,41], the combination of angular momentum conservation and translational velocity equilibrium [32], and the conservation of angular momentum [9], which is the method adopted in this study. For brevity, detailed calculations are not presented herein but can be found in Zhang et al. [9]. It is noted that classic treatment of rocking impact may provide unrealistically large estimate of energy dissipation for stocky

structures, whereas a recent study has adopted a Dirac-delta model to spread the impact effects over time and space [33]. However, the current study assumes that the use of different impact models will affect much more to the reproduction of entire time response history of a rocking structure, but much less the rocking seismic demand in a statistical point of view. Other than the abovementioned assumptions, the analytical model also holds its simplification in following aspects: (1) the two-dimensional planar model may underestimate the seismic responses of the real three-dimensional rocking bridges; (2) the model fits more neatly with the bridge behavior in the transverse direction, whereas a rocking frame should be expected for the bridge in the longitudinal direction; nevertheless, the rocking bridge is likely to have dominant responses in the transverse direction; (3) it needs more experimental investigations to confirm that different impact models will not affect significantly the column drift demand when viewed statistically; and (4) the current model changes the structural damping to be $\xi_n\sin(\alpha)$ (α is the slenderness angle that is calculated as $\tan^{-1}(b/H_e)$ in Fig. 1(b)) in the rocking response phase, which is more consistent with the rocking-mode damping ratios observed for small scale models [34]; however, large scale tests are needed to identify the correct rocking-mode damping for bridges.

2.2 Rocking Dynamics

The rocking behavior captured by the analytical model is illustrated with respect to a small-scale shaking-table test on a flexible rocking specimen in Truniger et al. [35]. The specimen has a fixed-base frequency of 1 Hz, a vibrational damping ratio of 0.16%, a slenderness angle α that equals 0.081, and a rocking frequency parameter f_r (calculated as $\sqrt{g/R}$ where R is $\sqrt{H_e^2+b^2}$ in Fig. 1(b)) that equals 3.22 Hz. The specimen is subjected to a symmetric Ricker-type excitation with a period of 1.0 s and a peak acceleration of 0.08g (i.e., the test is No. 10 in Table III in Truniger et al. [35]). Fig. 2 illustrates the rocking dynamics of the test specimen from both analytical model and shaking-table test, where the uplift response θ is normalized by the slenderness angle α, and the column drift response u is normalized by a displacement quantity u_{cr} that equals $g\tan(\alpha)/\omega_n^2$. As is seen, the dynamics of the system consist of low-frequency large magnitude rotations due to base uplift and high-frequency small perturbations due to column vibration. In general, the analytical model yields consistent uplift and column response predictions against the test results for the specimen considered herein.

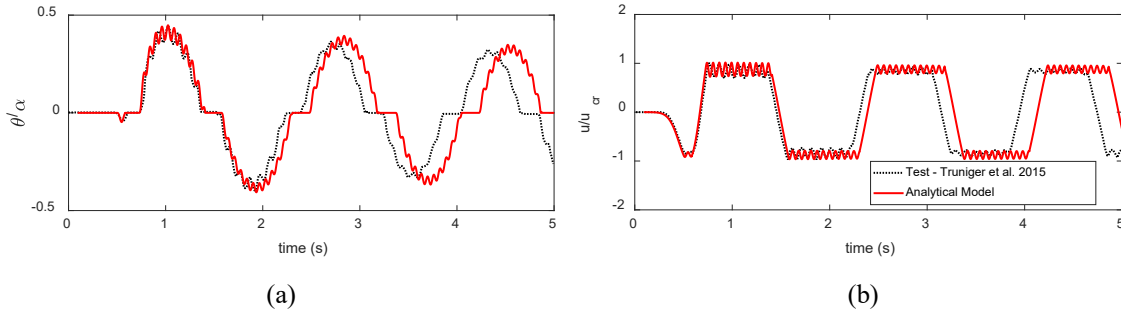(a)   (b)

Fig. 2 Rocking dynamics predicted by the analytical model when compared with test results (a) uplift response and (b) column vibrational response

However, rocking bridges respond to varying earthquakes with three possible conditions such as full contact, stabilized rocking and overturning. Fig. 3 illustrates these three conditions for a testbed bridge when subjected to pulse-type motions. The testbed is designed to have the bridge size R equals 6 m, and the slenderness angle α equals $\pi/9$ (20°). The rocking frequency parameter f_r turns out to be 1.28 rad/s. The flexible column has a vibrational natural frequency of 12.8 rad/s and a damping ratio of 5%. The rocking system is excited by cosine-type pulse motions with a variety of magnitude (a_p) and frequency (ω_p) parameters. As is depicted in Fig. 3, the rocking bridge responds distinctly as the input motions change. For instance, when the pulse motion features a large characteristic length (i.e., $2\pi^2 a_p/\omega_p^2$ as defined by [42]), the system will overturn with two different modes: model 1 with a single impact and mode 2 without impact [12,32]. On the other hand, the bridge will remain full contact and behaves as a single-DOF oscillator if the pulse motion is small in magnitude. Fig. 3 also indicates that the bridge responds to the majority of the pulse motions with a stabilized rocking behavior, under which a coupling of footing uplift and column vibration shall be expected. Fragility estimates that take into account these three different response conditions and the associated damage modes are the main subject of this study.

Time history analyses are carried out to investigate the dynamics of the rocking system under realistic ground

excitations. The abovementioned testbed bridge is designed to have the slenderness angle α equal $\pi/18$ (10°) and $\pi/9$ (20°), respectively. The ground motion is selected from the Pacific Earthquake Engineering Research (PEER) center ground motion database as the one recorded at the Transmitter Hill station during the 1983 Coalinga earthquake. Fig. 4 presents the acceleration history of the ground motion, and the uplift and drift responses of the testbed bridge. The column drift of the bridge with fixed-base condition is also presented for comparison purpose. It is noted that the column drift of rocking bridge is the total drift minus the rigid body motion due to foundation uplift, i.e., $H_e\theta$. As is indicated in Fig. 4(c), the rocking column behaves the same as a one-DOF oscillator in the first 2.7 seconds of time history. However, a considerable drift reduction can be achieved after rocking initiates. The column drift ratio is decreased from 1.32% to 0.70% for the case when α equals to 20°. The drift ratio can be further reduced to 0.28% if the system is more slender (i.e., when $\alpha = 10°$). The additional reduction of column drift for the more slender case is accompanied by the amplification of uplift angle ratio, θ/α, which is increased from 0.07 to 0.09 (Fig. 4(b)). As is seen, the use of rocking isolation reduces considerably the damage probability of column; whereas it introduces an additional damage mode associated with the rocking uplift, namely impact damage shall be expected at the pivotal locations if the pre-impact velocity is large.
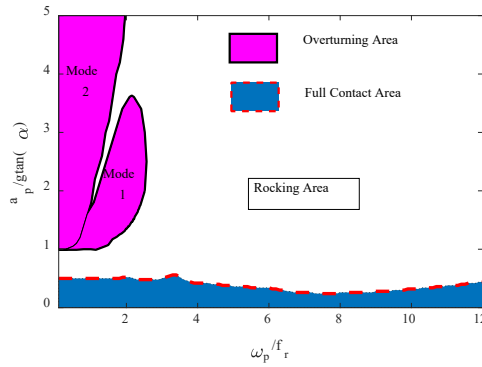

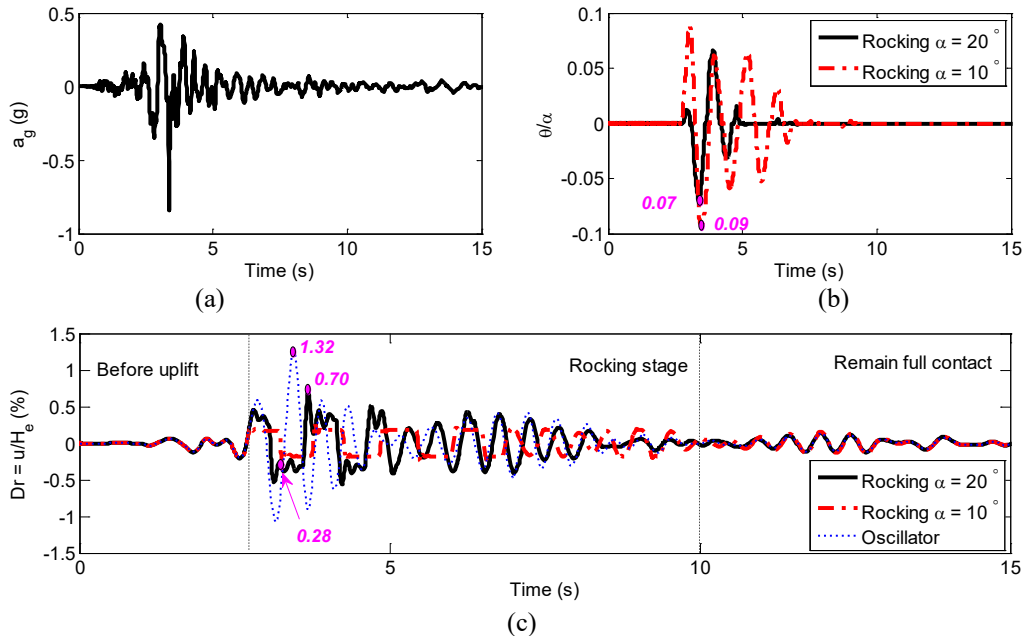Fig. 3 Three response conditions of the rocking system under pulse inputs

Fig. 4 Time history comparisons of the rocking system under a recorded motion: (a) ground motion acceleration history; (b) uplift angle responses of two rocking systems; and (c) column responses of the rocking systems and the oscillator

5

3. Probabilistic analysis framework of single-column rocking bridges

3.1 Rocking isolation of single-column bridge class

Influenced by the historic 1971 San Fernando earthquake, the design philosophies of California bridge columns have significantly changed since the earthquake event. Bridge columns designed prior to 1971 are much more susceptible to earthquake damage due to a lack of ductility. In this study, the single-column two-span and three-span continuous concrete box-girder bridge class designed in this era (i.e., prior to 1971) is considered as a testbed for rocking isolation. As shown in Fig. 1(a), a thorough plan review indicates that columns in this bridge class consist of three distinct shapes such as circular, oblong, and rectangular, where a mix of different sizes are designed for each shape [43]. As is listed in Table 1, geometric and material properties of this bridge class are based on an in-house database obtained from Caltrans together with a thorough review of bridge plans [43]. In addition to those listed in Table 1, parameters such as column diameter consist of discrete values with a certain percentage for each value (Fig. 5). Ideally, the footing width should be determined through an iterative process such that the rocking bridges are able to uplift and rock under small to moderate earthquakes, whereas they shall not overturn when subject to strong earthquakes. A tentative design with the footing width to column width ratio ($2b/b_c$) holding a uniform distribution between 1.2 and 1.8 is considered. Note that design requirement of this width ratio will be readdressed with the help of fragility estimates later in this study.

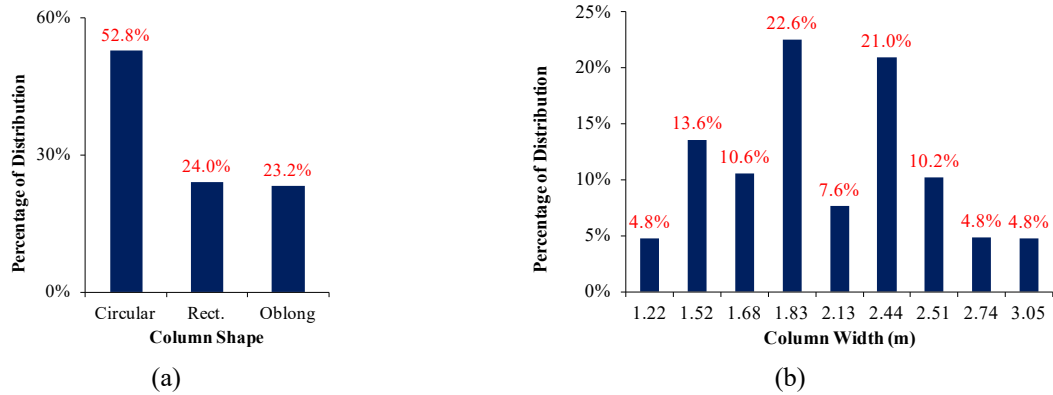(a)   (b)

Fig. 5 Discrete uncertainty distribution of independent parameters: (a) column shape; and (b) column width (from [43])

Table 1 Uncertain parameter distributions considered in the selected bridge class [44]

Parameter	Units	Distribution Type	μ	σ
Concrete compressive strength (f_c)	Mpa	Normal	29.03	3.59
Reinforcing steel yield strength (f_y)	Mpa	Lognormal	465	37.3
Longitudinal reinforcement ratio (ρ)	%	Uniform	2.25	0.52
Damping (ξ_n)	--	Normal	0.045	0.01
Span length				
Two-span (L_1)	m	Lognormal	31.78	8.74
Approach to main span ratio (three-span bridge) (L_2/L_1)	--	Normal	0.57	0.13
Deck width (B_d)	m	Lognormal	9.78	1.98
Deck depth-to-span ratio (H_d/L)	--	--	0.055	--
Column height (H)	m	Lognormal	6.63	0.87

Distributions of critical modeling parameters are examined through an experimental design using the Latin Hypercube Sampling (LHS) technique that samples 320 statistically significant yet nominally identical bridge cases. As shown in Fig. 6, the vibrational natural period T_n of columns holds a common range between 0.3 s and 1.2 s; the slenderness angle of rocking systems α spreads from $\pi/30$ (6°) to $\pi/8$ (22.5°); and the frequency parameter f_r is relatively concentrated between 1.0 rad/s and 1.3 rad/s. Distributions of these critical parameters reflect the realistic

ranges of rocking isolation design for the bridge class of concern. These distributions will be used to develop the fragility models in this study.
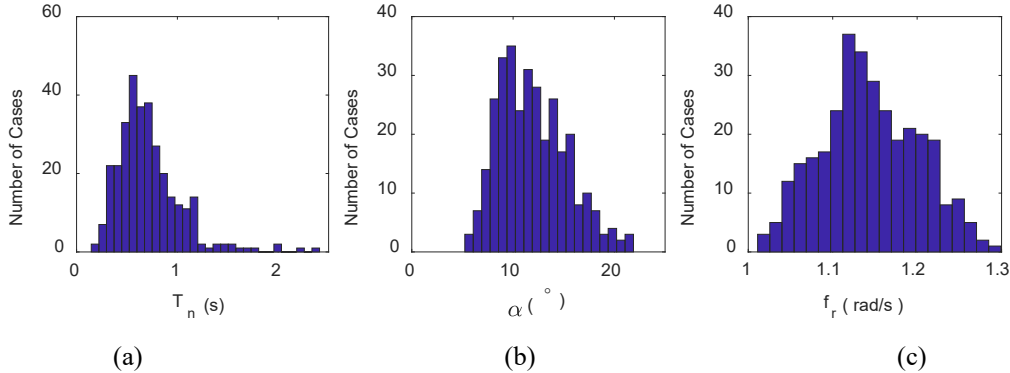

(a) (b) (c)

Fig. 6 Parameter distributions using LHS: (a) column natural period; (b) rocking slenderness angle; and (c) rocking frequency parameter

3.2 Selection of earthquake ground motions

640 ground motions are obtained by selecting and scaling 456 motions from the PEER center strong motion database. The obtained 640 time histories cover a wide range of ground motions that: (1) have earthquake magnitudes between 6.5 and 8.0 Mw; (2) feature both near-fault and far-field characteristics; and (3) would cause significant nonlinear behaviors on the fixed-base bridge columns. The selected 456 motions are scaled with respect to the spectral acceleration at 1.0s by a low scale factor between 0.80 and 1.20, whereas 184 motions are selected again and assigned with a scale factor between 1.25 and 2.50. Extremely large scale factors have not been used in this scaling process to preserve the kinematic features of the ground motions. Fig. 7 presents the distributions of some *IMs* of the ground motions. As is seen, ground motions vary significantly in terms of *PGA*, *PGV*, angular frequency corresponding to the largest pseudo spectral velocity (ω_v), and acceleration response spectra (S_a). The motions that feature large *IMs* are necessary in the current study to induce a relatively large number of overturning cases for the rocking bridges. The final set of 640 motions are randomly paired with the abovementioned 320 bridge samples, resulting in a probabilistic analysis framework that has one rocking bridge excited by two random motions.
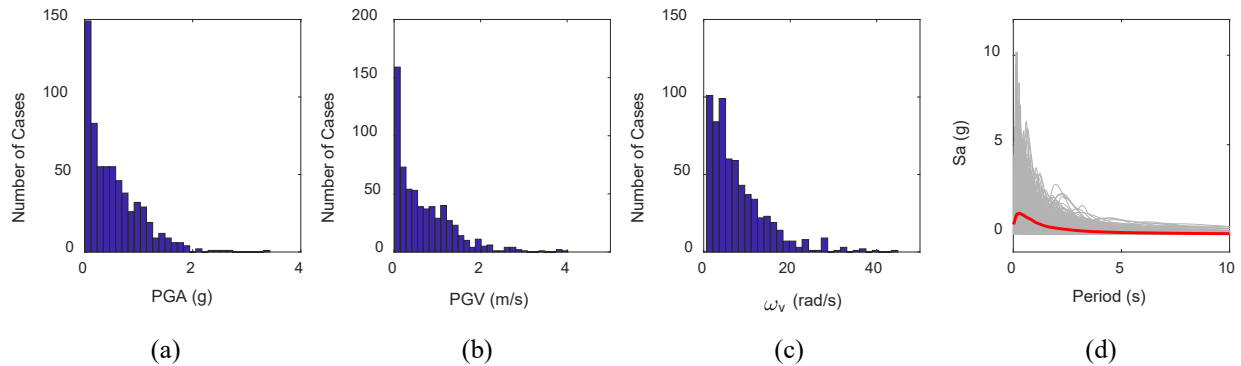

(a) (b) (c) (d)

Fig. 7 IM distributions of 640 ground motions: (a) *PGA*; (b) *PGV*; (c) ω_v; and (d) S_a

4.   Conditional probability damage models of the rocking bridges

4.1 Overall approach

Damage probabilities of the rocking bridges are conditional. As is depicted in Fig. 8, 178 out of 640 analysis cases remain full contact throughout earthquake excitations; 386 cases respond with a stabilized rocking behavior, while 76 cases overturn with unbounded responses. Fig. 8 essentially forms a two-layer categorization problem to classify (1) uplift versus non-uplift and (2) overturn versus non-overturn given that bridge uplifts. The first layer class probabilities are denoted as $P(U)$ and $P(FC) = 1 - P(U)$ for uplift and full contact (non-uplift) probabilities, respectively. Given the uplift condition, the second layer consists of $P(O|U)$ and $P(R|U) = 1 - P(O|U)$ to quantify overturning and stabilized rocking (non-overturning) probabilities, respectively. As such, the three response conditions of interest are full contact,

stabilized rocking, and overturning. Under these three response conditions, the vibrational damage of column is quantified through the engineering demand parameter (*EDP*) of column drift ratio. Given that (1) the rocking amplitude is easier to measure in real bridges than the pre-impact velocity; and (2) there exists a positive correlation between the rocking amplitude and the maximum pre-impact velocity, the *EDP* of uplift angle θ_{max} is adopted to assess the uplift impact damage. Thus, damage probabilities of the rocking system can be expressed as (1) $P(CD|FC)$ for column damage when conditional on the full contact condition; (2) $P(CD|R)$ and $P(ID|R)$ for column and impact damages, respectively, given that the system uplifts but does not overturn; and (3) 100% for both column and uplift damages when the system overturns. Therefore, the damage probability of each damage scenario can be calculated using the total probability theorem:

$$P_{\mathrm{C}} = P(\mathrm{FC})P(\mathrm{CD}|\mathrm{FC}) + P(\mathrm{U})P(\mathrm{R}|\mathrm{U})P(\mathrm{CD}|\mathrm{R}) + P(\mathrm{U})P(\mathrm{O}|\mathrm{U}) \times 100\%$$
$$= \left[1 - P(\mathrm{U})\right]P(\mathrm{CD}|\mathrm{FC}) + P(\mathrm{U})\left[1 - P(\mathrm{O}|\mathrm{U})\right]P(\mathrm{CD}|\mathrm{R}) + P(\mathrm{U})P(\mathrm{O}|\mathrm{U}) \times 100\% \tag{5}$$

$$P_{\mathrm{I}} = P(\mathrm{U})P(\mathrm{R}|\mathrm{U})P(\mathrm{ID}|\mathrm{R}) + P(\mathrm{U})P(\mathrm{O}|\mathrm{U}) \times 100\%$$
$$= P(\mathrm{U})\left[1 - P(\mathrm{O}|\mathrm{U})\right]P(\mathrm{ID}|\mathrm{R}) + P(\mathrm{U})P(\mathrm{O}|\mathrm{U}) \times 100\% \tag{6}$$

$$P_{\mathrm{O}} = P(\mathrm{U})P(\mathrm{O}|\mathrm{U}) \tag{7}$$

where P_{C}, P_{I}, and P_{O} are the probabilities of column damage, impact damage and system overturning, respectively. The response classes, and damage modes, locations, and descriptions of the rocking bridges are summarized in Table 2.

Table 2 Definition of rocking bridges' response classes, and damage modes, locations, and descriptions

| Response Class		Damage mode	Damage location	Damage description
Full contact (FC)		Column damage (CD)	Column plastic-hinge zones	Concrete cracking, spalling, core concrete shedding and crushing, transverse steel loss, longitudinal bars buckling, fracture, etc.
Uplift (U)	Stabilized rocking (R)	Column damage (CD)		
		Impact damage (ID)	Footing bottom, pivotal locations	Concrete cracking, spalling, shedding, and crushing; damage to exposed reinforcements
	Overturning	Bridge overturn (O)	Complete damage for both column and footing	
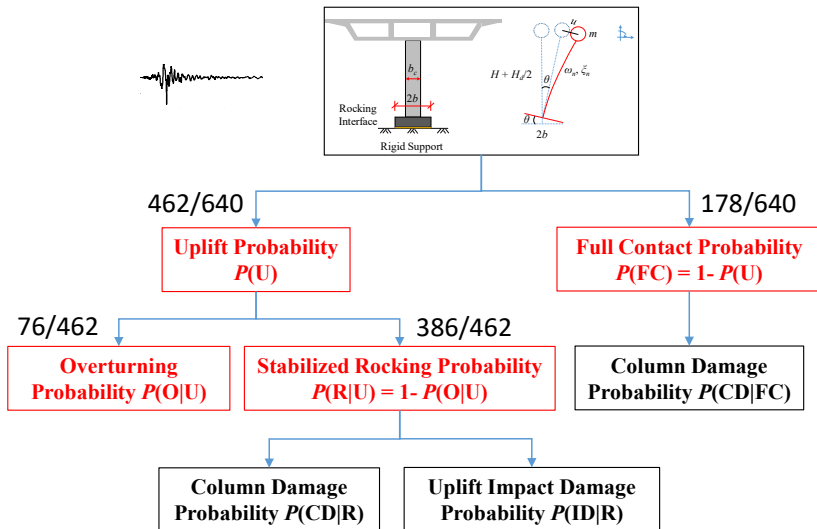
Fig. 8 Probability analysis diagram for the rocking bridges

A multi-step machine learning framework is set up to develop the fragility models associated with each conditional probability. As shown in Fig. 9, response conditions (e.g., full contact or overturning) and the associated peak seismic demands (e.g., column drift ratio u_{max}/H_e and normalized uplift angle θ_{max}/α) are considered to be correlated to the influential parameters. The parameters (referred to as predictors) of interest come from three sources such as the ground motion IMs, the rocking parameters (i.e., the frequency parameter f_r and slenderness angle α), and the column vibrational parameters (i.e., vibrational natural frequency ω_n and damping ratio ξ_n). It is worth mentioning that various ground motion IMs have been taken into account in the machine learning framework, including both intensity and frequency parameters. The intensity parameters consist of peak ground acceleration (PGA), peak ground velocity (PGV), peak ground displacement (PGD), cumulative absolute velocity (CAV), cumulative absolute displacement (CAD), spectral accelerations and velocities at 0.2 and 1.0 seconds, respectively, Arias intensity (I_A), and velocity intensity (I_V), whereas the frequency parameters include the frequency at the largest spectral acceleration (ω_p), the frequency at the largest spectral velocity (ω_v), PGA/PGV, and PGV/PGD. This study adopts a generalized linear model (GLM) to link the system responses to the predictors:

$$y = \beta^T \mathbf{X} + \varepsilon \tag{8}$$

where y is the response vector, β^T is the coefficient vector, $\mathbf{X} = \{x_1, x_2, \ldots, x_m\}$ is the set of influential parameters, and ε is the error vector representing the differences between the exact and predicted values of y. The model error is assumed to be a normally distributed random variable with a zero mean [45]. The most influential parameters are determined through stepwise regression, which identifies the best fitting subset of predictor variables by sequentially adding and removing terms from the proposed GLM based on a given statistical criterion, such as F-statistic or goodness of fit [46]. Engineering judgement is also used in this step to (1) avoid overfitting by introducing too many similar predictors, such as ω_p (i.e., frequency corresponding to the largest pseudo spectral acceleration) and PGA/PGV; and (2) incorporate those predictors that would affect the response in a physically reasonable way (e.g., the slenderness angle α shall bear a negative influence on the uplift response of the rocking system).

For categorization probabilities such as $P(U)$ and $P(O|U)$, the response vector y is assigned with a binomial distribution (e.g., 0 for full contact responses and 1 for uplift cases), which allows the GLM shown in Eq. (8) to be transformed to a logistic regression function:

$$\Pr(y = 1 | \mathbf{X}) = \frac{e^{\beta^T \mathbf{X}}}{1 + e^{\beta^T \mathbf{X}}} \tag{9}$$

where $\Pr(y=1|\mathbf{X})$ is the logistic function that is assigned into binary values with a boundary of 0.5 in the current study (e.g., the rocking system is predicted to uplift if $\Pr > 0.5$, while the system remains full contact if $\Pr < 0.5$). The soundness of the developed logistic models for $P(U)$ and $P(O|U)$ is further evaluated by the five-fold cross-validation method using the metrics of accuracy and recall. Accuracy defines the fraction of the correctly predicted cases over the total data space, while recall is the fraction of the correctly predicted uplift (or overturning) cases over the total true uplift (or overturning) cases. In addition, given that much fewer overturning cases have occurred (76 overturning cases out of 462 uplifted cases), the prediction of overturning probability $P(O|U)$ faces the imbalanced data problem, which is tackled by assigning a weight factor for the minor class (i.e., the overturning class) to increase the misclassification cost with respect to overturning [47]. A sensitivity study is carried out to identify the optimal weight factor that yields a proper balance between accuracy and recall ratios. Iterations have been carried out until satisfactory $P(U)$ and $P(O|U)$ predictions have been identified.

For regression probabilities $P(CD|FC)$, $P(CD|R)$, and $P(ID|R)$, the response vector y and predictor vector $\mathbf{X}$ shown in Eq. (8) are transformed into the natural logarithm space, which is consistent with the derivation of the probabilistic seismic demand models (PSDMs) for fragility estimates [48,49]. As such, the GLM shown in Eq. (8) produces metamodels for the target $EDPs$, i.e., the drift ratio u_{max}/H_e and the normalized uplift angle θ_{max}/α, as functions of the influential parameters identified from the stepwise regression. Both the dispersion of model error ε and the goodness of fit are checked for each metamodel by the five-fold cross-validation method. In the metamodel assessment, p-$values$ are computed to interpret the results of the hypothesis test [50], where smaller p-$values$ indicate more evidence to reject the null hypothesis (i.e., the hypothesis that there is no relationship between the predictor and response). p-$values$ associated with the explanatory functions are controlled to be smaller than 0.05, assuring that the final predictors included in the model are indeed not selected by chance. The final metamodels are further convolved with the capacity models for each EDP through a Monte Carlo analysis for developing the conditional probability estimates of $P(CD|FC)$, $P(CD|R)$, and $P(ID|R)$. In the model development, every parameter is in the international system of

units. In particular, each regressive metamodel is derived to have the same dimension as the corresponding target *EDP*.
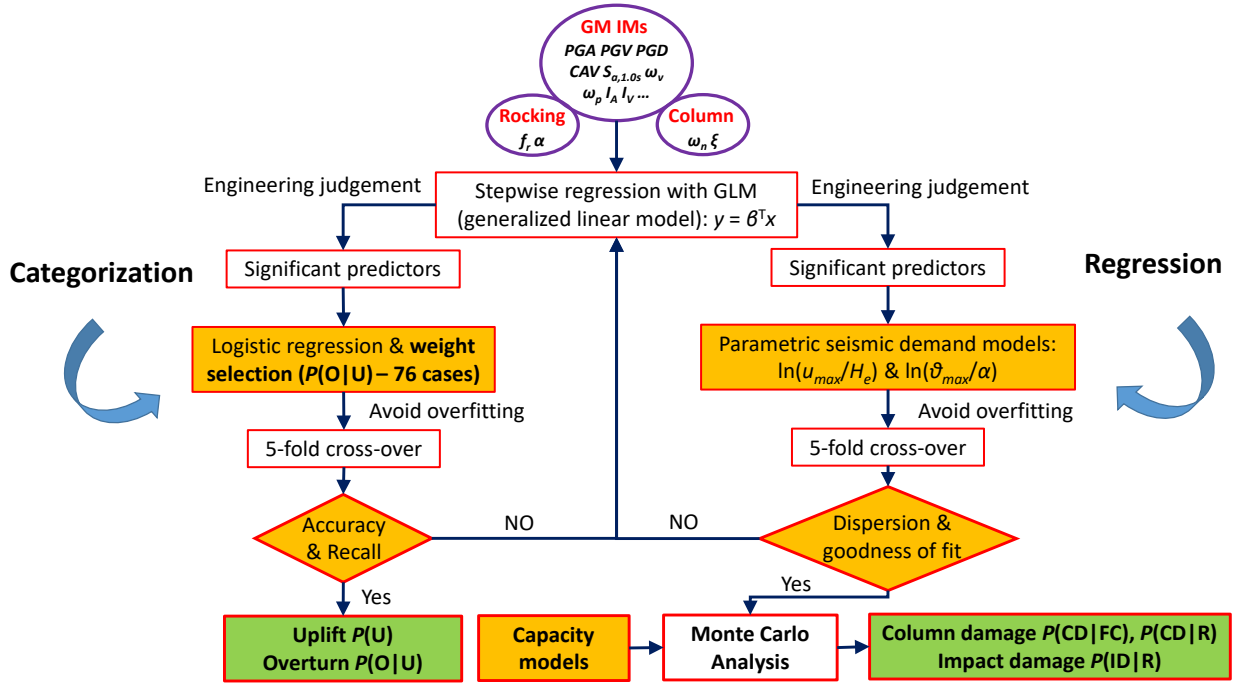

Fig. 9 Machine learning framework for the development of rocking fragility models

4.2 Uplift probability P(U) and overturning probability P(O|U)

Uplift occurs when the moment generated by the peak inertial force exceeds the resisting moment provided by gravity, which can be equivalently transformed to be the condition when $S_{a,Tn}$ is bigger than $g\tan(\alpha)$. Herein, $S_{a,Tn}$ stands for the ground motion's response spectral acceleration at the natural period of the fixed-base bridge (T_n). To this end, unless dynamic analyses have been conducted beforehand for each bridge sample to obtain its natural period, T_n, $S_{a,Tn}$ cannot be conveniently computed. On the other hand, the machine learning framework identifies that the predictor of $\ln\left(\dfrac{PGV}{g\tan\alpha}\right)$ is one of the most significant ones that can yield accurate predictions on the uplift probability. In addition, as will be discussed later, the ground motion *IM* of *PGV* has also been identified as the significant predictor for other rocking mode responses, which would in general favor the development and comparisons of the system fragility curves. The multi-step machine learning framework identifies the following logistic regression function to classify uplift versus full contact:

$$P(\mathrm{U}) = \frac{e^{8.51+3.33\ln\left(\frac{PGV}{g\tan\alpha}\right)}}{1+e^{8.51+3.33\ln\left(\frac{PGV}{g\tan\alpha}\right)}} \tag{10}$$

The five-fold cross-validation indicates that the logistic function of Eq. (10) bears an average accuracy rate of 94% and recall rate of 96%. Fig. 10(a) shows the logistic function prediction when slenderness angle is changing, where the numerical data from 640 analyses are also presented for comparison purpose. As is depicted, the rocking system is more apt to uplift when the system becomes more slender, i.e., when α is smaller. In general, the uplift tendency predicted by the logistic function (Eq. (10)) is consistent with that shown from the numerical data. For instance, numerical data indicate that the rocking bridges uplift almost inevitably when *PGV* of the ground motion is larger than 0.4 m/s, at which uplift probabilities predicted by Eq. (10) are also larger than 0.5 for all cases.
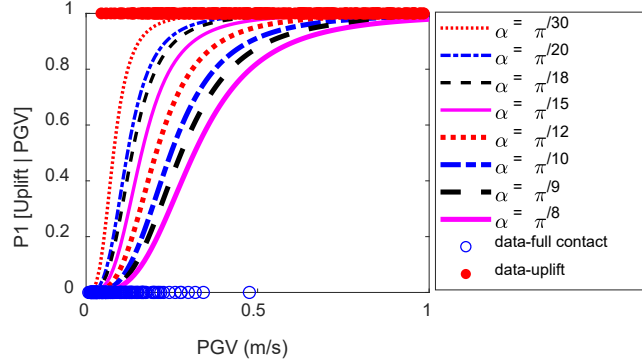
Fig. 10 Logistic regression to predict the uplift probability $P(U)$ with various slenderness angle of α

A relatively more challenging task lies in the prediction of overturning probability $P(O|U)$. Using multiple stripe analysis together with the maximum likelihood concept, previous studies have identified that the overturning probability of rigid rocking structures can be reasonably predicted when it is conditioned on the dimensionless *IM* of $\frac{f_r PGV}{g \tan \alpha}$ [36,37]. This study utilizes a different approach, i.e., the machine learning framework with the logistic regression method, but also identifies that $\ln\left(\frac{f_r PGV}{g \tan \alpha}\right)$ is the best predictor among various parameters. As previously mentioned, given that fewer overturning cases have occurred, the study assigns a weight factor on each overturning case to increase its miss-classified cost. Sensitivity studies are conducted to pinpoint the proper weight factor that can have a satisfactory balance between accuracy and recall of the prediction. Fig. 11 presents the prediction performance with respect to different normalized weight factors (i.e., weight factor normalized by the ratio between the number of stabilized rocking cases (n_1) and the number of overturning cases (n_2)). As shown from the figure, the recall of overturning cases increases from 0.4 to 1.0 when larger weight factors are assigned, while the accuracy of the overall correct predictions decreases at the same time (i.e., changing from around 0.9 to 0.6). The weight factor is chosen to produce a performance balance point, which is defined to be a point that has very close accuracy and recall rates at the same time. The balance point of around 0.81 of accuracy and recall is identified in this study, at which the associated weight factor is selected as $0.9 n_1/n_2$. The resultant logistic regression function to predict rocking overturning turns out to be:

$$P(O|U) = \frac{e^{1.50 + 3.92 \ln\left(\frac{f_r PGV}{g \tan \alpha}\right)}}{1 + e^{1.50 + 3.92 \ln\left(\frac{f_r PGV}{g \tan \alpha}\right)}} \tag{11}$$
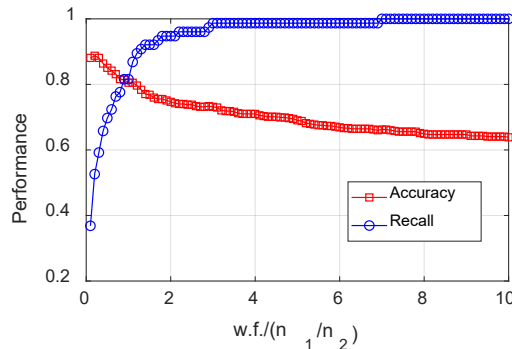

Fig. 11 The influence of weight factor on the performance of overturning prediction

The use of Eq. (11) to predict rocking overturning yields an average accuracy and recall of 81% by the five-fold cross-validation method. Note that the performance of overturning prediction can be improved if a response surface model is adopted (i.e., instead of using a generalized linear function, one can adopt the logistic regression with a second-degree polynomial function to predict overturning). However, given that the relatively limited data of

overturning cases do not offer enough observations to justify the use of higher-order metamodels, GLM is still preferred in this study to avoid overfitting. Logistic function predictions are presented in Fig. 12 for the sample bridge with $\alpha = \pi/15$ and $f_r = 1.1$ rad/s, where the numerical data of stabilized rocking and overturning cases are also shown. The widespread of logistic functions with respect to different slenderness angles (Fig. 12(a)) has emphasized its importance of stabilizing the rocking behavior of the system. The system overturning tendency can be significantly reduced should a wider footing (i.e. the larger α value) is designed. It is also promising to observe that the general range reflected by the numerical data concurs with that predicted by the logistic function. Fig. 12(b) also indicates that the bigger the size of the rocking bridge (i.e., the smaller the f_r value), the smaller the overturning probability that can be expected.
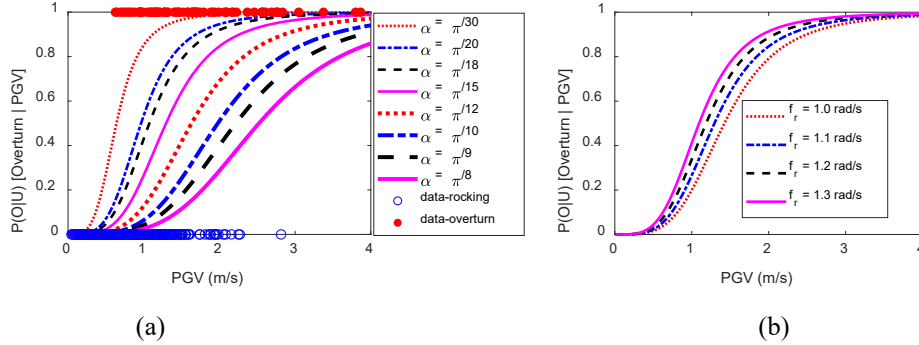

(a)   (b)

Fig. 12 Logistic regression to predict the overturning probability p_2 (a) with various slenderness angle of α; and (b) with various frequency parameter of f_r

4.3 Column and impact conditional damage probabilities P(CD|FC), P(CD|R), and P(ID|R)

Under each response condition, damage probabilities are assessed with respect to column and footing impact. Parametric PSDMs are developed for column drift ratio u_{max}/H_e and normalized uplift angle θ_{max}/α, respectively, by using stepwise regression together with the GLM. For the demand model of column drift ratio under full contact condition (i.e., the demand model for estimating $P(CD|FC)$), the stepwise regression identifies that the most influential predictor is $\ln\left(\dfrac{PGV}{\omega_n H_e}\right)$; and the machine learning procedure results in the following metamodel:

$$\ln\left(\frac{u_{\max}}{H_e}\right)\bigg|_{Full\ Contact} = -0.41 + 0.90\ln\left(\frac{PGV}{\omega_n H_e}\right) + \varepsilon_{P(CD|FC)} \tag{12}$$

The accuracy of the column drift model under the full contact condition and the *p-values* associated with the model's significant predictor are presented in Table 3. The model yields a five-fold cross validated *R*-square value of 0.81, a model error with 0.18 as the variance, and less-than-0.0001 *p-values* for the predictor of $\ln\left(\dfrac{PGV}{\omega_n H_e}\right)$. The accuracy of this model is also presented in Fig. 13, where the predicted values are plotted against the actual data. Fig. 13 shows that the PSDM is acceptable in predicting the target response. It is noted that the drift demand during full contact is found to be mainly influenced by the peak ground velocity of the ground motions. Other motion parameters, such as the frequency parameter ω_p, have shown to bear small influences on the drift responses, which seems to be counter-intuitive. This is because the full contact response condition requires the ground excitations to be small in magnitude, short in the dominant period, or non-pulse like in general. Such requirement excludes typical pulse-type strong motions whose frequency content ω_p would significantly affect the drift responses of a one-DOF oscillator. As proof, the *p-values* for the parameter of $\ln(\omega_p)$ is 0.25 herein, which is bigger than 0.05 and is much larger than the *p-values* for $\ln\left(\dfrac{PGV}{\omega_n H_e}\right)$. In addition, the derived PSDM shown in Eq. (12), along with other parametric PSDMs derived in this study, is dimensionally consistent. In these PSDMs, the predictors identified on the right hand side and the *EDPs* on the left side are both dimensionless.

The PSDM is further convolved with the column capacity model to develop the conditional probability estimate

of $P(CD|FC)$. The damage states defined by HAZUS [51] (i.e., slight, moderate, extensive, and collapse) are considered as a guideline to determine the corresponding limit values for column damage, where the limit state of column drift ratio to reach each state is selected from the study by Yi et al. [52]. According to Yi et al. [52], the median column drift ratio limits are 0.7%, 1.5%, 2.5%, and 5% for reaching slight, moderate, extensive, and complete damage states, respectively. In addition, the capacity limit states are assumed to possess lognormal distributions with a dispersion of 0.35. To this end, the PSDM and capacity model of column drift ratio are convolved into the fragility estimate of $P(CD|FC)$ using a Monte Carlo analysis: (1) at each PGV level, generate 10^6 demand estimates of column drift ratio; (2) sample 10^6 capacity estimates for a specific damage state from the corresponding limit state distribution; (3) generate a binary survive-failure vector for the column by comparing the seismic demand and capacity estimates; and (4) calculate the occurrence ratio of failure events as the $P(CD|FC)$ estimate at given PGV level. Fig. 14 presents the estimates of the slight column damage probability given the full contact condition, where fragility curves corresponding to the column with an effective height of 7.9 m and five different natural frequency cases are developed. It is evident from the figure that the column vibrational damage probabilities decrease as the column becomes more rigid (i.e., as ω_n increases). As previously discussed, the damage probability $P(CD|FC)$ is subjected to the full contact response condition, which is usually in association of small-magnitude or non-pulse type earthquake excitations and relatively stocky rocking bridges. Therefore, the probability of the full contact column damage, which can be calculated as $[1- P(U)]\cdot P(CD|FC)$, is essentially very small.

Table 3 Performance of the *PSDM* of column drift ratio given full contact condition

Model	Five-fold CV R^2	Model error $\varepsilon_{P(CD|FC)}$	p-values $\ln\left(\dfrac{PGV}{\omega_n H_e}\right)$
Eq. (12)	0.81	$N(0, 0.18)$	*

*: less than 0.0001
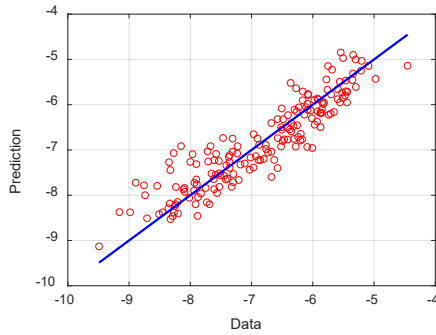
Fig. 13 *PSDM* prediction vs actual numerical data of $\ln(u_{max}/H_e)$ for the full contact condition
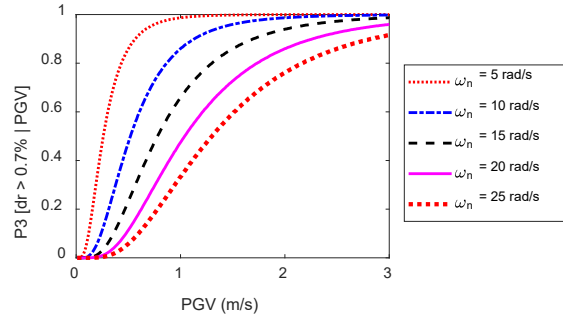
Fig. 14 Column slight damage probability $P(CD|FC)$ that is conditioned on the full contact response condition

Under the stabilized rocking response condition, bridges respond to the seismic excitations with a coupled behavior of column vibration and footing uplifting, associated with which are two coexisting damage modes: the column damage and uplift impact damage. Similarly, the PSDM is developed for the column drift ratio u_{max}/H_e under the rocking response condition, which yields the following metamodel:

$$\ln\left(\frac{u_{\max}}{H_e}\right)\bigg|_{Rocking} = 0.13 + 0.77\ln\left(\frac{g\tan\alpha}{\omega_n^2 H_e}\right) + 0.36\ln\left(\frac{PGV}{f_r H_e}\right) + \varepsilon_{P(CD|R)} \qquad (13)$$

The performance of column drift model and the associated *p-values* of the two identified influential predictors are listed in Table 4, which indicates that the model has a five-fold cross validated *R*-square value of 0.89, a normally distributed model error with 0.03 as the variance, and less-than-0.0001 *p*-values for both predictors of $\ln\left(\dfrac{g\tan\alpha}{\omega_n^2 H_e}\right)$

and $\ln\left(\dfrac{PGV}{f_r H_e}\right)$. It is noted that the ground motion parameter of PGV is still observed to perform better than other intensity parameters such as the PGA. Fig. 15 also illustrates good accuracy of the $PSDM$ by plotting the predicted responses from Eq. (13) against the actual data of $\ln(u_{max}/H_e)$ under the rocking response condition. Using the same Monte Carlo analysis strategy, the conditional damage probability $P(CD|R)$ is developed with respect to the slight damage state for the sample bridge that has $f_r = 1.1$ rad/s, $\alpha = \pi/15$, and $\omega_n = 10$ rad/s. Figs. 16(a) and 16(b) present the fragility estimates of $P(CD|R)$ when the system slenderness angle and vibrational natural frequency are changing, respectively. Fig. 16(a) shows that column damage probability amplifies when the system slenderness angle α increases, resulting from the fact that the larger slenderness angle will reduce the rocking uplift response more, which makes the system behaves closer to a SDOF oscillator. On the other hand, Fig. 16(b) emphasizes that the flexibility of the column bears significant influences on the column damage probability once rocking is initiated. Especially, a comparison between Fig. 16(b) and Fig. 14 concludes that column flexibility is much more crucial to increase or decrease column damage when rocking behavior is triggered. This phenomenon results from the fact that the rocking motion significantly alters the dynamics of column vibration. Modal and uplift analyses of the rocking system indicate that the column would vibrate along an approximate magnitude level of u_{cr} that equals $g\tan(\alpha)/\omega_n^2$ with a modal frequency of $\omega_n/\sin(\alpha)$ [9,29,32,41]. As such, column drift demand under the rocking response condition can be roughly considered to be affected by ω_n in the power of two, which is much more significant than the full contact case.

Table 4 Performance of the $PSDM$ of column drift ratio given rocking condition

Model	Five-fold CV R^2	Model error $\varepsilon_{P(CD|R)}$	$\ln\left(\dfrac{g\tan\alpha}{\omega_n^2 H_e}\right)$	$\ln\left(\dfrac{PGV}{f_r H_e}\right)$
			p-values
Eq. (13)	0.89	$N(0, 0.03)$	*	*

*: less than 0.0001

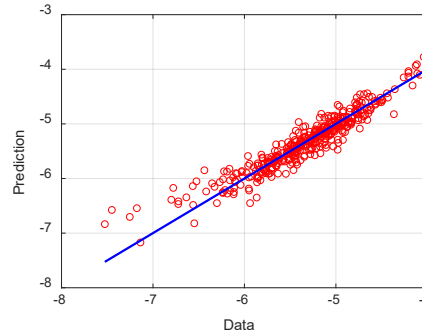Fig. 15 PSDM prediction vs actual numerical data of $\ln(u_{max}/H_e)$ for the rocking response condition
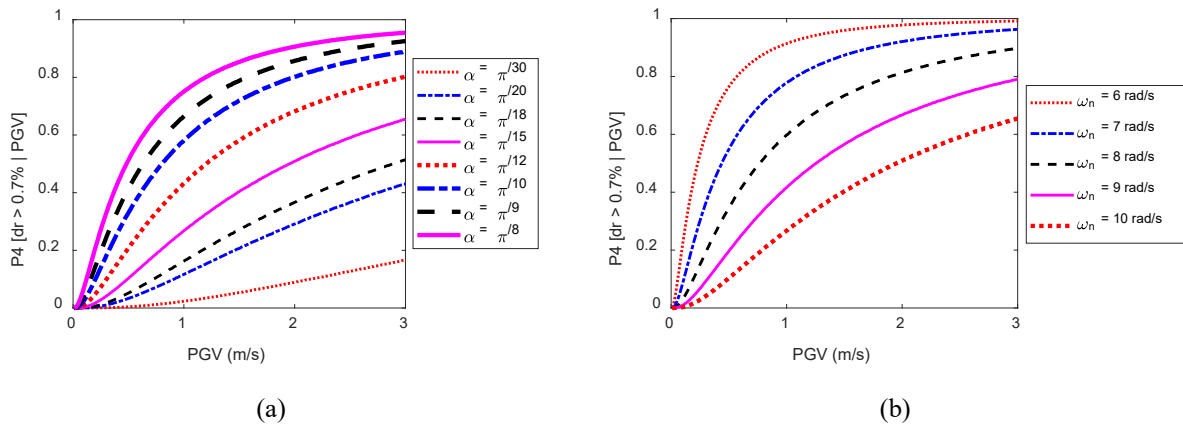

(a)   (b)

Fig. 16 Column damage probability $P(CD|R)$ that is conditioned on the rocking condition (a) with various slenderness angle of α; and (b) with various vibrational frequency parameter of ω_n

The prediction of rocking uplift responses is of the main interest of recent studies that investigate the dynamics of rocking structures [30,36–38]. In these studies, various ground motion *IMs* have been compared in terms of their efficiency and sufficiency to correlate to the rocking uplift demand. A similar task is conducted in this study with the help of machine learning framework, where stepwise regression identifies that the velocity components of ground motions are more efficient (i.e., bigger *R*-square values and smaller errors) and sufficient (i.e., smaller *p-values*) to predict the maximum rocking response. The observed better performance of ground motion velocity components in predicating rocking response is consistent with those identified from previous studies [30,36,37]. In particular, a recent study has pinpointed that the duration-based ground motion *IMs*, such as t_{uni}, the summation of the time intervals and CAV_2, the time integral of the absolute ground acceleration, both during which the ground acceleration exceeds a specific threshold, have dominant importance on rocking uplift demand [37]. Fig. 17 illustrates the definition of CAV_2 for a particular record, where the threshold is selected as $g\tan(\alpha)$ that triggers the rocking motion of a rigid block. In this study, the PSDM of normalized uplift demand is proposed as a function that consists of three ground motion *IMs* such as ω_v, *PGV* and CAV_2, and two rocking parameters that are f_r and α. The dimensionless *PSDM* has the following closed-form expression:

$$\ln\left(\frac{\theta_{max}}{\alpha}\right)\bigg|_{Rocking} = 0.97 - 2.66\ln\left[\left(\frac{\omega_v}{f_r}\right)^{0.3} + \left(\frac{f_r}{\omega_v}\right)^{0.7}\right] - 1.43\ln(\tan\alpha)$$
$$+ 0.15\ln\left(\frac{f_r CAV_2}{g}\right) + 1.18\ln\left(\frac{f_r PGV}{g}\right) + \varepsilon_{P(ID|R)}$$
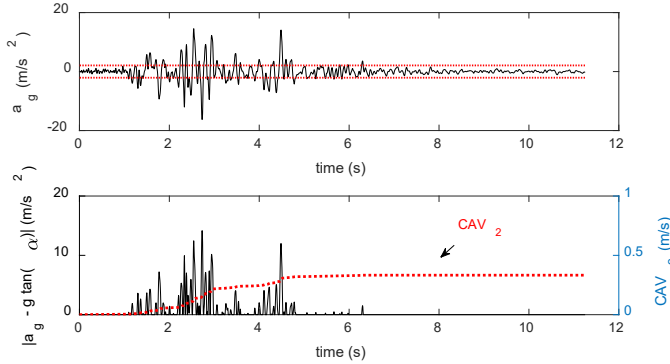
(14)

Fig. 17 Cumulative absolute velocity of the ground motion that triggers the rocking motion (CAV_2)
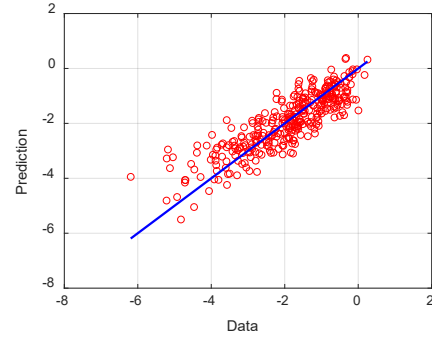

Fig. 18 PSDM prediction vs actual numerical data of $\ln(\theta_{max}/\alpha)$ for the rocking response condition

The performance of uplift demand model and the associated *p-values* of the identified four influential predictors are listed in Table 5. The model has a five-fold cross validated *R*-square value of 0.72, a normally distributed model error with 0.40 as the variance, and less-than-0.0001 *p-values* for all four significant predictors. Fig. 18 also illustrates good accuracy of the PSDM by plotting predicted responses from Eq. (14) against actual data of $\ln(\theta_{max}/\alpha)$ under the rocking response condition. It is also promising to observe from Fig. 18 that the model provides close predictions for the large uplift angle cases (i.e., when θ_{max} approachs α, or equally when $\ln(\theta_{max}/\alpha)$ is close to 0). In this study, the uplift impact damage is considered to be substantial as the maximun rocking angle reaches one fourth of the slendernes angle, α [53]. Therefore, the capacity model is selected to have a lognormal distribution with the median of $\theta_{max}/\alpha =$ 0.25 and a dispersion of 0.35. A Monte Carlo analysis is carried out with respect to the conditional damage probability $P(ID|R)$ for the sample bridge that has $\alpha = \pi/15$, $f_r = 1.1$ rad/s, $\omega_v = 5f_r$, and $CAV_2 = 3$ m/s. Fig. 19 presents the fragility estimates of $P(ID|R)$ when each of the influential parameters is changing. Fig. 19(a) confirms that the uplift impact damage probability is affected substantially by the slenderness of the system, namely the increase of slenderness angle α would reduce greatly the impact damage. A larger size of the rocking bridges (when f_r is reduced in Fig. 19(b)) is also observed to be able to lower the damage probability of $P(ID|R)$. The influence from ω_v, the dominant frequency of the ground motion spectral velocity, is evaluated in Fig. 19(c), where much larger damage probabilities occur when ω_v stays in the range of one to five times of the rocking frequency parameter, f_r. Fig. 19(d) also demonstrates the

considerable impact from the ground motion duration-based *IM* of CAV_2.

Table 5 Performance of the *PSDM* of uplift angle under rocking condition

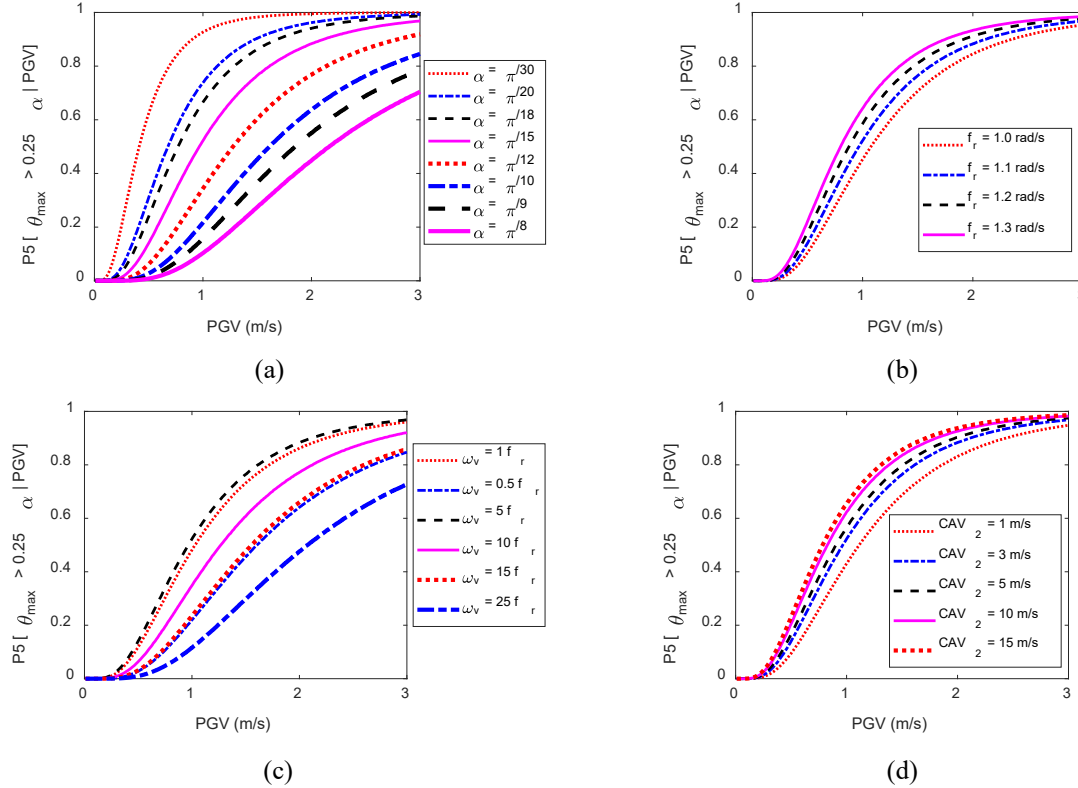| Model	Five-fold CV R^2	Model error $\varepsilon_{P(ID\|R)}$	*p-values*			
			$\ln\left[\left(\dfrac{\omega_v}{f_r}\right)^{0.3} + \left(\dfrac{f_r}{\omega_v}\right)^{0.7}\right]$	$\ln(\tan\alpha)$	$\ln\left(\dfrac{f_r CAV_2}{g}\right)$	$\ln\left(\dfrac{f_r PGV}{g}\right)$
Eq. (14)	0.72	$N(0, 0.40)$	*	*	*	*

*: less than 0.0001

(a)

(b)

(c)

(d)

Fig. 19 Uplift damage probability $P(ID|R)$ with various (a)slenderness angle of α; (b) rocking frequency parameter of f_r; (c) frequency of spectral velocity, ω_v; and (d) cumulative absolute velocity of exceedance, CAV_2

5. Fragility estimates and design rationale of rocking bridges

The abovementioned conditional probabilities form the basis to develop the fragility estimates for the rocking bridges. Additionally, a practically more meaningful question lies in whether the rocking isolation proposed in the current study is seismically more resilient than the as-built design (i.e., with the fixed-base condition). To this end, rocking bridge fragility curves conditioned only on ground motion *IMs* are compared with the ones calculated for the as-built bridge columns. Under full contact and stabilized rocking conditions, damage probabilities of the rocking column are considered to be very small and are only assessed with respect to the slight damage state. However, rocking columns are considered to have complete damage when overturning happens. Fragility curves of rocking bridges are directly calculated using the total probability theorem that is shown in Eqs. (5), (6) and (7), while a numerical analysis procedure is carried out for the fragility estimates of as-built bridges: (1) construct 640 two-dimensional finite element models for the bridges shown in Fig. 1(a), where fiber section elements and concentrated mass are used to simulate the nonlinear behavior of column and the inertia effect of deck, respectively; (2) develop a parametric PSDM of column drift ratio using the proposed machine learning framework; and (3) conduct a Monte Carlo analysis to calculate the fragility curves by convolving the demand model with the column drift capacity model that is suggested by Yi et al. [52]. The PSDM of as-built columns is given in Eq. (15). The model has a five-fold cross-validated *R*-square value of 0.90, a model error with 0.35 as the dispersion, and smaller-than-0.0001 *p-values* for all the predictors. Fig. 20 also

illustrates the accuracy of the PSDM by plotting the predicted responses against the actual numerical data.

$$\ln\left(\frac{u_{max}}{H_e}\right)\Big|_{As-built} = 3.92 + 1.11\ln\left(\frac{PGV}{\omega_n H_e}\right) - 0.86\ln\left(\frac{\omega_p}{\omega_n} + \frac{\omega_n}{\omega_p}\right)$$

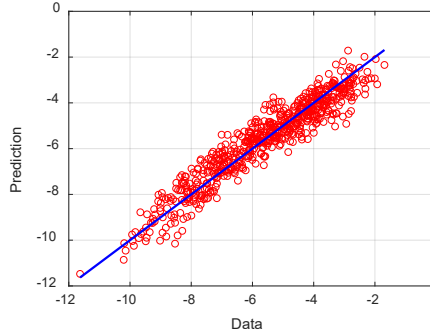$$+ 0.50\ln\left(\frac{g}{\omega_n^2 H_e}\right) - 0.25\ln(\xi_n) + \varepsilon_{As-built} \tag{15}$$

Fig. 20 PSDM prediction vs actual numerical data of $\ln(u_{max}/H_e)$ for the fixed-base bridge columns

The fragility estimates of rocking bridges consist of three potential damage modes: column damage with respect to the slight state, uplift damage with respect to $\theta_{max}/\alpha = 0.25$, and overturning of the system, whereas fragility curves of the fixed-base columns are assessed at four different damage states (i.e., DS1 for slight, DS2 for moderate, DS3 for extensive, and DS4 for collapse) that are defined by HAZUS [51]. It is noted that the DS4 state corresponds to column collapsing, at which the fixed-base columns are expected to lose their axial capacities, and the as-built bridges are expected to completely lose their traffic carrying capacities. Repair actions for the DS4 state consist of the replacement of the entire bridge, and a very long-term traffic closure. In addition, previous experimental results indicate that the column drift ratio with a 5% median and a lognormal dispersion of 0.35 is adequate to quantify the column collapsing state. Hence, the DS4 state for as-built columns are considered to result in equivalent damage consequences as the overturning for rocking bridges.

Fig. 21 presents the fragility comparisons between rocking bridges and as-built fixed-base columns for the sample cases that have: (1) $f_r = 1.1$ rad/s, $\omega_n = 10$ rad/s, $\xi_n = 4.5\%$, $\omega_p = 20$ rad/s, $\omega_v = 5f_r$, and $CAV_2 = 3$ m/s; and (2) the previously-observed most important rocking parameter, the slenderness angle α changes from $\pi/30$ to $\pi/8$. Fig. 21 in general conveys the following: (1) rocking isolation can reduce significantly the column slight damage probabilities when compared with the fixed-base cases; (2) the slenderness angle designed for the sample cases has a critical point of $\pi/15$, below which the probability of rocking overturning is higher than the failure probability of as-built columns; however, much lower overturning failure probability can be expected for the rocking bridges when slenderness angles are larger than $\pi/12$; (3) as the slenderness angle increases, smaller uplift and overturning probabilities can be expected; however, the column damage probability will first reduce because of the smaller overturning probability, but then increase because the system behaves closer to a SDOF oscillator. The slenderness angle for the sample cases has an overall optimal range between $\pi/15$ and $\pi/10$, among which rocking bridges yield both lower overturning tendencies and considerably reduced column damage probabilities. Fig. 21 proves that the rocking isolation design proposed in this study can be seismically much more resilient than as-built bridges when the system slenderness angle is carefully designed.
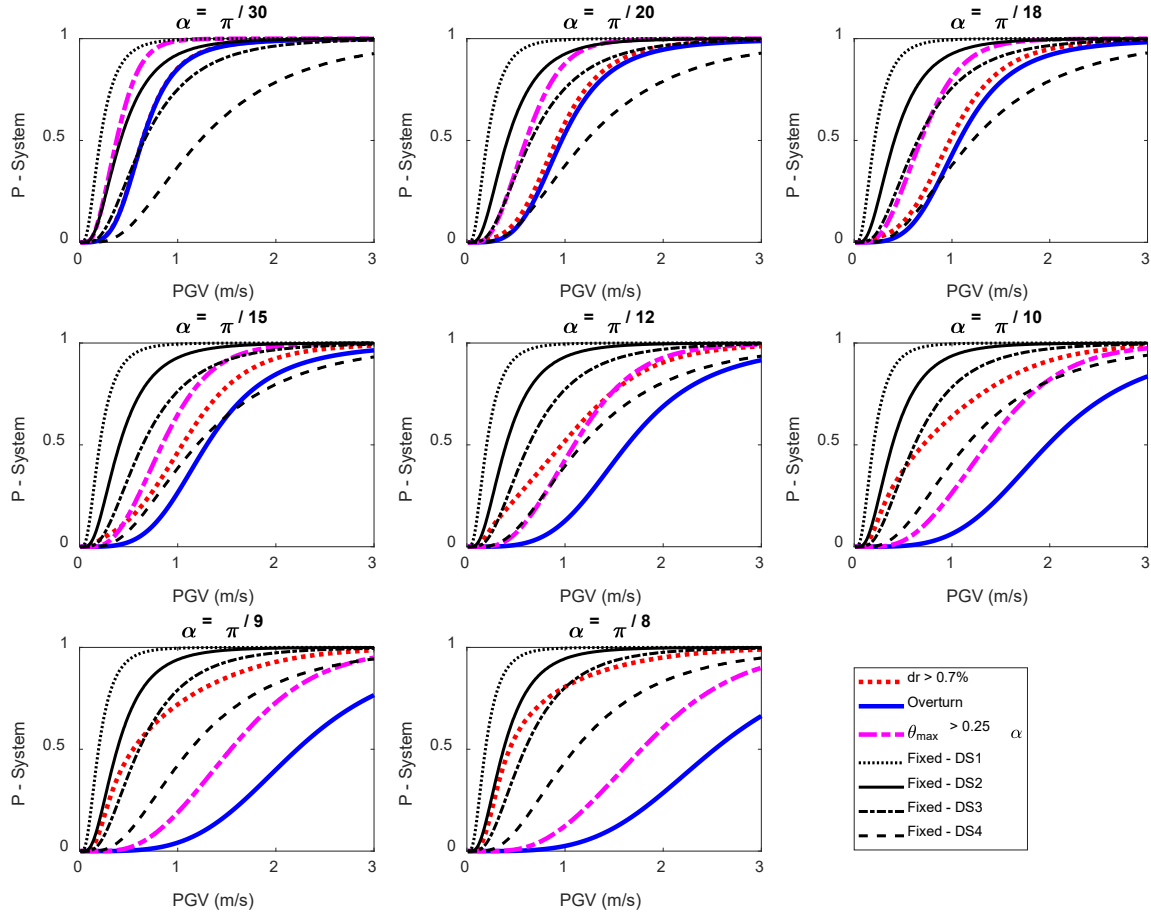
Fig. 21 Fragility comparisons between rocking bridges and as-built bridges with fixed-base condition

6. Conclusions

The rationale of the rocking isolation concept is assessed through fragility estimates with respect to the single-column highway bridge class in California that is designed prior to 1971. A probabilistic analysis framework is proposed to capture various response conditions and damage modes associated with rocking bridges. Subsequently, an iterative multi-step machine learning methodology is developed to predict the associated class and conditional damage probabilities. The soundness and requirement of the rocking isolation design are further assessed by comparing the rocking fragility curves with those of fixed-base bridges. The following conclusions can be drawn from this study:

1. Rocking bridges respond to varying levels of earthquake excitations with distinct response conditions such as full contact, stabilized rocking, and overturning. This study proposes a two-layer metamodel framework to estimate first the response class probabilities and then the second-layer conditional damage probabilities, which offers a viable approach for the fragility analysis of rocking bridges.
2. The uplift and overturning probabilities of the rocking bridges are greatly affected by the velocity component of the ground motion and the rocking parameters such as the slenderness angle α and the rocking frequency parameter f_r. The logistic regression functions identified from the machine learning framework yield physically reasonable and numerically consistent uplift and overturning predictions.
3. The rocking motion significantly alters the dynamics of the column vibration. First, a more stocky system would cause the column to behave closer to a SDOF oscillator, which would amplify the column drift demand. Moreover, column damage under the rocking condition is generally affected by its natural frequency in the power degree of two, which is much more significant than the fixed-base case.
4. The uplift demand of the rocking bridges is influenced by multiple ground motion parameters; the intensity measure of PGV, the velocity frequency measure of ω_v, and the duration-based measure of CAV_2. The rocking parameters (i.e., the slenderness angle and the rocking frequency parameter) also bear substantial influences

on the rotational demand.

5. Fragility comparisons between rocking bridges and as-built columns validate the use of rocking isolation to reduce column damage. However, judicious consideration should be placed on the rocking design parameter of slenderness angle α, which is suggested to be in the range between $\pi/15$ and $\pi/10$ for the sample bridges. In this angle range, lower overturning tendencies and greatly reduced column damage probabilities can be achieved simultaneously.

In summary, the study explores the seismic performance of the rocking bridges in a probabilistic manner. The derived fragility curves address the general question whether rocking bridges can be seismically more resilient than conventional designs. On the other hand, the developed logistic regression models and dimensionally consistent parametric PSDMs are specific to the single-column rocking bridges discussed in this study, namely the models may cause larger errors when structures with totally different sizes or configurations are of concern. A more advanced numerical analysis method or more rational column capacity models for the rocking bridges may also change the specific values in this study. However, the overall framework and methodology, and the general conclusions shed light on a way to assess and design the rocking isolation to improve the seismic resilience of single-column highway bridges.

7. Acknowledges

References

1. Ugalde JA, Kutter BL, Jeremić B. Rocking response of bridges on shallow foundations. *PEER Report, Pacific Earthquake Engineering Research Center, Universityof California, Berkeley, CA* 2010; **101**.

2. Deng L, Kutter BL, Kunnath SK. Probabilistic seismic performance of rocking-foundation and hinging-column bridges. *Earthquake Spectra* 2012; **28**(4): 1423–1446. DOI: 10.1193/1.4000093.

3. Deng L, Kutter BL, Kunnath SK. Seismic design of rocking shallow foundations: displacement-based methodology. *Journal of Bridge Engineering* 2014; **19**(11): 04014043. DOI: 10.1061/(ASCE)BE.1943-5592.0000616.

4. Antonellis G, Panagiotou M. Seismic response of bridges with rocking foundations compared to fixed-base bridges at a near-fault site. *Journal of Bridge Engineering* 2014; **19**(5): 04014007. DOI: 10.1061/(ASCE)BE.1943-5592.0000570.

5. Agalianos A, Psychari A, Vassiliou MF, Stojadinovic B, Anastasopoulos I. Comparative assessment of two rocking isolation techniques for a motorway overpass bridge. *Frontiers in Built Environment* 2017; **3**: 1–19. DOI: 10.3389/fbuil.2017.00047.

6. Kutter BL, Moore M, Hakhamaneshi M, Champion C. Rationale for shallow foundation rocking provisions in ASCE 41-13. *Earthquake Spectra* 2016; **32**(2): 1097–1119. DOI: 10.1193/121914EQS215M.

7. Gajan S, Kutter BL. Capacity, settlement, and energy dissipation of shallow footings subjected to rocking. *Journal of Geotechnical and Geoenvironmental Engineering* 2008; **134**(8): 1129–1141. DOI: 10.1061/(ASCE)1090-0241(2008)134:8(1129).

8. Anastasopoulos I, Gazetas G, Loli M, Apostolou M, Gerolymos N. Soil failure can be used for seismic protection of structures. *Bulletin of Earthquake Engineering* 2010; **8**(2): 309–326. DOI: 10.1007/s10518-009-9145-2.

9. Zhang J, Xie Y, Wu G. Seismic response predictions of bridges with rocking column-foundation. *Earthquake Engineering & Structural Dynamics* 2019(48): 152–170. DOI: 10.1002/eqe.3129.

10. Konstantinidis D, Makris N. Seismic response analysis of multidrum classical columns. *Earthquake Engineering and Structural Dynamics* 2005; **34**(10): 1243–1270. DOI: 10.1002/eqe.478.

11. Housner GW. The behavior of inverted pendulum structures during earthquakes. *Bulletin of the Seismological Society of America* 1963; **53**(2): 403–417. DOI: 10.1017/CBO9781107415324.004.

12. Zhang J, Makris N. Rocking response of free-standing blocks under cycloidal pulses. *Journal of Engineering Mechanics* 2001; **127**: 473–483.

13. Dimitrakopoulos EG, DeJong MJ. Overturning of retrofitted rocking structures under pulse-yype excitations.

Journal of Engineering Mechanics 2012; **138**(8): 963–972. DOI: 10.1061/(ASCE)EM.1943-7889.0000410.

14. Vassiliou MF, Makris N. Analysis of the rocking response of rigid blocks standing free on a seismically isolated base. *Earthquake Engineering & Structural Dynamics* 2012; **41**: 177–196. DOI: 10.1002/eqe.1124.

15. Makris N, Vassiliou MF. Planar rocking response and stability analysis of an array of free-standing columns capped with a freely supported rigid beam. *Earthquake Engineering & Structural Dynamics* 2013; **42**: 431–449. DOI: 10.1002/eqe.2222.

16. Bachmann JA, Vassiliou MF, Stojadinovic B. Dynamics of rocking podium structures. *Earthquake Engineering & Structural Dynamics* 2017; **46**: 2499–2517. DOI: 10.1002/eqe.2915.

17. Vassiliou MF, Burger S, Egger M, Bachmann JA, Broccardo M, Stojadinovic B. The three-dimensional behavior of inverted pendulum cylindrical structures during earthquakes. *Earthquake Engineering & Structural Dynamics* 2017; **46**: 2261–2280. DOI: 10.1002/eqe.2903.

18. Makris N, Aghagholizadeh M. The dynamics of an elastic structure coupled with a rocking wall. *Earthquake Engineering & Structural Dynamics* 2017; **46**: 945–962. DOI: 10.1002/eqe.2838.

19. Chatzis MN, Espinosa MG, Smyth AW. Examining the Energy Loss in the Inverted Pendulum Model for Rocking Bodies. *Journal of Engineering Mechanics* 2017; **143**(5): 4017013. DOI: 10.1061/(ASCE)EM.1943-7889.0001205.

20. Giouvanidis AI, Dimitrakopoulos EG. Nonsmooth dynamic analysis of sticking impacts in rocking structures. *Bulletin of Earthquake Engineering* 2017; **15**(5): 2273–2304. DOI: 10.1007/s10518-016-0068-4.

21. Kalliontzis D, Sritharan S, Schultz A. Improved coefficient of restitution estimation for free rocking members. *Journal of Structural Engineering* 2016; **142**(12): 06016002. DOI: 10.1061/(ASCE)ST.1943-541X.0001598.

22. Prieto F, Lourenco PB, Oliveira CS. Impulsive Dirac-delta forces in the rocking motion. *Earthquake Engineering and Structural Dynamics* 2004; **33**(7): 839–857. DOI: 10.1002/eqe.381.

23. Makris N, Konstantinidis D. The rocking spectrum and the limitations of practical design methodologies. *Earthquake Engineering and Structural Dynamics* 2003; **32**(2): 265–289. DOI: 10.1002/eqe.223.

24. Lipscombe BPR, Pellegrino S. Free rocking of prismatic blocks. *Journal of Engineering Mechanics* 1993; **119**(7): 1387–1410.

25. Ma QTM. The mechanics of rocking structures subjected to ground motion. The University of Auckland, 2010.

26. Pena F, Prieto F, Lourenco PB, Costa AC, Lemos J V. On the dynamics of rocking motion of single rigid-block structures. *Earthquake Engineering & Structural Dynamics* 2007; **36**: 2383–2399. DOI: 10.1002/eqe.739.

27. Bachmann JA, Jost C, Studemann Q, Vissiliou MF, Stojadinovic B. An analytical model for the dynamic response of an elastic SDOF system fixed on top of a rocking single-story frame structure: experimental validation. *ECCOMAS Congress, Crete Island, Greece,* 2016. DOI: 10.3929/ETHZ-B-000225616.

28. Oliveto G, Calio I, Greco A. Large displacement behaviour of a structural model with foundation uplift under impulsive and earthquake excitations. *Earthquake Engineering and Structural Dynamics* 2003; **32**(3): 369–393. DOI: 10.1002/eqe.229.

29. Vassiliou MF, Mackie KR, Stojadinovic B. Dynamic response analysis of solitary flexible rocking bodies: modeling and behavior under pulse-like ground excitation. *Earthquake Engineering & Structural Dynamics* 2014; **43**: 1463–1481. DOI: 10.1002/eqe.2406.

30. Acikgoz S, DeJong MJ. The rocking response of large flexible structures to earthquakes. *Bulletin of Earthquake Engineering* 2014; **12**(2): 875–908. DOI: 10.1007/s10518-013-9538-0.

31. Vassiliou MF, Truniger R, Stojadinovic B. An analytical model of a deformable cantilever structure rocking on a rigid surface: development and verification. *Earthquake Engineering & Structural Dynamics* 2015; **44**: 2775–2794. DOI: 10.1002/eqe.2608.

32. Acikgoz S, DeJong MJ. The interaction of elasticity and rocking in flexible structures allowed to uplift. *Earthquake Engineering & Structural Dynamics* 2012; **41**: 2177–2194. DOI: 10.1002/eqe.2181.

33. Acikgoz S, DeJong MJ. Analytical modelling of multi-mass flexible rocking structures. *Earthquake Engineering & Structural Dynamics* 2016; **45**: 2103–2122. DOI: 10.1002/eqe.2735.

34. Truniger R, Vassiliou MF, Stojadinovic B. Experimental study on the interaction between elasticity and rocking. *Proceedings of the 10th National Conference in Earthquake Engineering*, Anchorage, AK: Earthquake Engineering Research Institute; 2014. DOI: 10.4231/D38911R5S.

35. Truniger R, Vissiliou MF, Stojadinovic B. An analytical model of a deformable cantilever structure rocking on a rigid surface: experimental validation. *Earthquake Engineering & Structural Dynamics* 2015; **44**: 2795–2815. DOI: 10.1002/eqe.2609.

36. Dimitrakopoulos EG, Paraskeva TS. Dimensionless fragility curves for rocking response to near-fault excitations. *Earthquake Engineering & Structural Dynamics* 2015; **44**: 2015–2033. DOI: 10.1002/eqe.2571.

37. Giouvanidis AI, Dimitrakopoulos EG. Rocking amplification and strong-motion duration. *Earthquake*

Engineering and Structural Dynamics 2018: 1–22. DOI: 10.1002/eqe.3058.

38. Bachmann JA, Strand M, Vassiliou MF, Broccardo M, Stojadinović B. Is rocking motion predictable? *Earthquake Engineering and Structural Dynamics* 2018; **47**(2): 535–552. DOI: 10.1002/eqe.2978.

39. Ebad Sichani M, Padgett JE, Bisadi V. Probabilistic seismic analysis of concrete dry cask structures. *Structural Safety* 2018; **73**: 87–98. DOI: 10.1016/j.strusafe.2018.03.001.

40. Bakhtiary E, Gardoni P. Probabilistic seismic demand model and fragility estimates for rocking symmetric blocks. *Engineering Structures* 2016; **114**: 25–34. DOI: 10.1016/j.engstruct.2016.01.050.

41. Chopra AK, Yim SC -S. Simplified earthquake analysis of structures with foundation uplift. *Journal of Structural Engineering* 1985; **111**(4): 906–930. DOI: 10.1061/(ASCE)0733-9445(1985)111:4(906).

42. Makris N, Black CJ. Dimensional analysis of rigid-plastic and elastoplastic structures under pulse-type excitations. *Journal of Engineering Mechanics* 2004; **130**(9): 1006–1018. DOI: 10.1061/(ASCE)0733-9399(2004)130:9(1006).

43. Mangalathu S. Performance based grouping and fragility analysis of box-girder bridges in California. Georgia Institute of Technology, 2017.

44. Mangalathu S, Jeon JS, Padgett JE, DesRoches R. ANCOVA-based grouping of bridge classes for seismic fragility assessment. *Engineering Structures* 2016; **123**: 379–394. DOI: 10.1016/j.engstruct.2016.05.054.

45. Dobson AJ. *An introduction to generalized linear models*. Chapman & Hall/CRC; 2002.

46. James G, Witten D, Hastie T, Tibshirani R. *An Introduction to Statistical Learning - with Applications in R*. Springer Texts in Statistics; 2013.

47. He H, Garcia EA. Learning from imbalanced data. *IEEE Transactions on Knowledge and Data Engineering* 2009; **21**(9): 1263–1284. DOI: 10.1109/TKDE.2008.239.

48. Xie Y, Zhang J. Optimal design of seismic protective devices for highway bridges using performance-based methodology and multiobjective genetic optimization. *Journal of Bridge Engineering* 2017; **22**(3): 04016129. DOI: 10.1061/(ASCE)BE.1943-5592.0001009.

49. Xie Y, Zhang J. Design and optimization of seismic isolation and damping devices for highway bridges based on probabilistic repair cost ratio. *Journal of Structural Engineering* 2018; **144**(8): 04018125. DOI: 10.1061/(ASCE)ST.1943-541X.0002139.

50. Hines WW, Montgomery DC, Goldsman DM, Borror CM. *Probability and statistics in engineering*. 4th Ed. Wiley, Hoboken, N.J.; 2003.

51. FEMA. *Multi-hazard loss estimation methodology, earthquake model, HAZUS-MH MR1, advanced engineering building module, technical and user's manual*. Department of Homeland Security Emergency Preparedness and Response Directorate, FEMA; 2003.

52. Yi JH, Kim SH, Kushiyama S. PDF interpolation technique for seismic fragility analysis of bridges. *Engineering Structures* 2007; **29**(7): 1312–1322. DOI: 10.1016/j.engstruct.2006.08.019.

53. Singh KP, Ph D, Soler AI, Ph D, Smith M, International H. Predicting the structural response of free-standing spent fuel storage casks under seismic events. *Transactions, SMiRT 16*, Washington DC: 2001.